Production of warm ions in electron beam generated E × B plasma ⊘

Nirbhav Singh Chopra ⓘ ; Ivan Romadanov ⓘ ; Yevgeny Raitses ✉ ⓘ

Check for updates

View Online   Export Citation

Articles You May Be Interested In

Plasma atomic layer etching of SiO_2 with a low global warming potential fluorocarbon precursor (C_6F_6)

J. Vac. Sci. Technol. A (April 2024)

Plasma atomic layer etching of SiO_2 and Si_3N_4 with heptafluoropropyl methyl ether ($C_3F_7OCH_3$)

J. Vac. Sci. Technol. A (February 2020)

Spatial distributions of the absolute CF and CF 2 radical densities in high-density plasma employing low global warming potential fluorocarbon gases and precursors for film formation

J. Vac. Sci. Technol. A (September 2001)

Production of warm ions in electron beam generated E × B plasma

View Online   Export Citation   CrossMark

Nirbhav Singh Chopra,[1,2] (iD) Ivan Romadanov,[1] (iD) and Yevgeny Raitses[1,a] (iD)

AFFILIATIONS

[1]Princeton Plasma Physics Laboratory, Princeton University, Princeton, New Jersey 08543, USA
[2]Department of Astrophysical Sciences, Princeton University, Princeton, New Jersey 08544, USA

Note: This paper is part of the Special Topic: Plasma Sources for Advanced Semiconductor Applications.
[a]Author to whom correspondence should be addressed: yraitses@pppl.gov

ABSTRACT

Several recent experiments have demonstrated low-damage processing of 2D materials, such as graphene and single crystal diamond, using electron beam (e-beam) generated plasmas with applied crossed electric and magnetic (E × B) fields. The low damage of these sensitive materials is commonly attributed to the low energy of ions incident to the substrate surface and the ion confinement in E × B fields. In this work, measurements of atom and ion velocity distribution functions in an e-beam E × B plasma at sub-mTorr argon pressures using a laser-induced fluorescence diagnostic revealed the presence of a warm population of ions with temperatures of ~ 1 eV that are sufficient to destroy the ion confinement in E × B fields and drive the ion flux by cross field diffusion in the direction opposite to the applied electric field, toward the plasma-bounded walls or substrate. Thus, it is this nearly ambipolar diffusion process that is responsible for the flux of charged particles impinging on the wall/substrate surface.

Published under an exclusive license by AIP Publishing. https://doi.org/10.1063/5.0189707

Electron beam (e-beam) generated plasmas with applied crossed electric and magnetic fields (E × B) are promising for applications requiring generation of ions and radicals for processing in low pressure environments.[1–3] For material processing applications, a key capability of such magnetically confined e-beam plasma sources is that they can generate reactive species while maintaining a flux of low energy particles to substrates placed in the periphery of the plasma region.[4,5] Such remote low temperature plasma sources have already demonstrated their applicability for atomic scale[6,7] and nanomaterial processing.[1]

Similar to many E × B plasma systems, such as Penning discharges, Hall discharges, and sputtering magnetrons, the electron cross field transport in the e-beam generated E × B plasmas can be anomalous, driven by the formation of large-scale plasma structures and scattering of electrons on plasma fluctuations.[8–11] However, ions are usually unmagnetized, and therefore, their transport is dominated by the electric field and collisions with neutrals. Previous work on e-beam generated E × B plasmas has demonstrated the formation of an ion-confining electric potential well.[1,8,9] This potential well can be leveraged for low-damage threshold material processing applications by limiting ion flux, thereby preventing energetic ions from damaging material surfaces. In this Letter, we investigate the electron and ion transport in a partially magnetized e-beam plasma source with applied

E × B fields and report on the formation of a warm ion population that can overcome this confining potential.

The experimental setup is shown in Fig. 1. It consists of a cylindrical vacuum chamber of radius $R_{ch} = 10$ cm. The chamber is pumped to a base pressure of $\sim 1\ \mu$Torr and then filled to a pressure of 0.1 mTorr by flowing Ar gas through a needle valve. On one end of the cylindrical chamber, an electron emitting thermionic cathode is mounted, consisting of an ohmically heated filament made from a tungsten wire of diameter 0.4 mm. The exposed part of the cathode wire is about 1 cm in length, and it is biased to a potential $V_C = -55$ V that is negative relative to the grounded chamber (anode). Therefore, electrons emitted by the cathode are accelerated in the plasma-cathode sheath and injected into the chamber as a beam-like nonthermal electron population. These electrons collide with the neutral gas atoms, ionizing them and forming ions and bulk plasma electrons with lower energies than the beam electrons. An axial magnetic field (B = 100 G) is generated by electromagnets arranged in a pseudo-Helmholtz configuration along the chamber, providing radial confinement of the beam and bulk electrons. The cathode is mounted on a floating ceramic break, such that the cathode is electrically isolated from the grounded chamber. Therefore, a circular area of the wall with radius 1.75 cm directly behind the cathode filament is electrically

13 December 2024 12:43:00
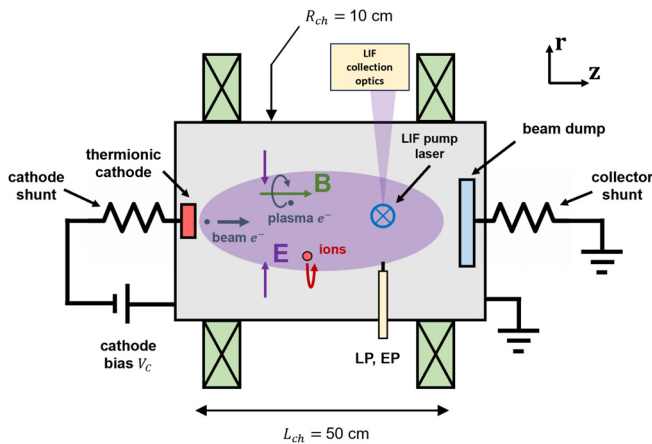
FIG. 1. Schematic of experimental setup and diagnostics used in these experiments. The shunt resistors placed in series with the cathode and collector measure the current sourced by the cathode and collector, respectively. For the LIF diagnostic, the argon ion Ar II $3d^4F_{9/2}$ metastable state is pumped at an excitation wavelength of 664.55 nm, with fluorescence signal emitted at 434.93 nm.[12] For argon neutrals, the Ar I $4s\,^2P^0_{3/2}$ state is pumped at an excitation wavelength of 667.91 nm, with fluorescence signal emitted at 750.59 nm.[13]

floating, preventing electron loss to the wall behind the cathode. Similar to previously investigated e-beam plasma source configurations, either with electron emitting thermionic,[9] ion induced secondary electron emission,[2] or RF plasma[8] cathodes, the described source has an electron collecting anode plate on the opposite end of the cathode, such that the cathode and collector are separated a distance $L_{ch} = 50$ cm. Both cathode and collector are axially aligned such that they are intersected by the same magnetic field lines.

The results of diagnostics measurements are shown in Fig. 2. Cylindrical Langmuir probe (LP) and floating emissive probe (EP) diagnostics are used to determine the radial dependence of the electron energy distribution function $f(\varepsilon)$ (EEDF), electron density n_e, electron temperature T_e, and plasma potential V_{pl} in the discharge.[14,15] The EEDF is also used to calculate the spatial dependence of ionization rate constant K_{iz}, which is given by

$$K_{iz} = \frac{1}{n_e} \left(\frac{2}{m_e} \right)^{1/2} \int_0^\infty d\varepsilon \, \sigma_{iz}(\varepsilon) \varepsilon^{\frac{1}{2}} f(\varepsilon), \qquad (1)$$

where σ_{iz} is the ionization cross section for electrons impact ionization of argon.[16] The radial dependence of the electron density, electron temperature, plasma potential, and ionization rate constant are shown in Figs. 2(a) and 2(b). Electron density and temperature reach 3×10^9 cm^{-3} and 11 eV at the center of the discharge ($r = 0$ cm). In the region of $r < 2$ cm, a radial potential well of approximately 1 V is formed, creating a radially inward electric field of nearly 0.5 V/cm. Most ions are also produced in this well region.

Determining the ion temperature is critical to understanding the radial ion flux, which can be directed to a substrate with materials sensitive to ion-induced damage (e.g., graphene or diamond). The argon ion velocity distribution function (IVDF) was determined by laser induced fluorescence (LIF) diagnostic at two radial locations where the signal-to-noise ratio was acceptable. The LIF diagnostic was additionally used to determine the argon neutral VDF to investigate the
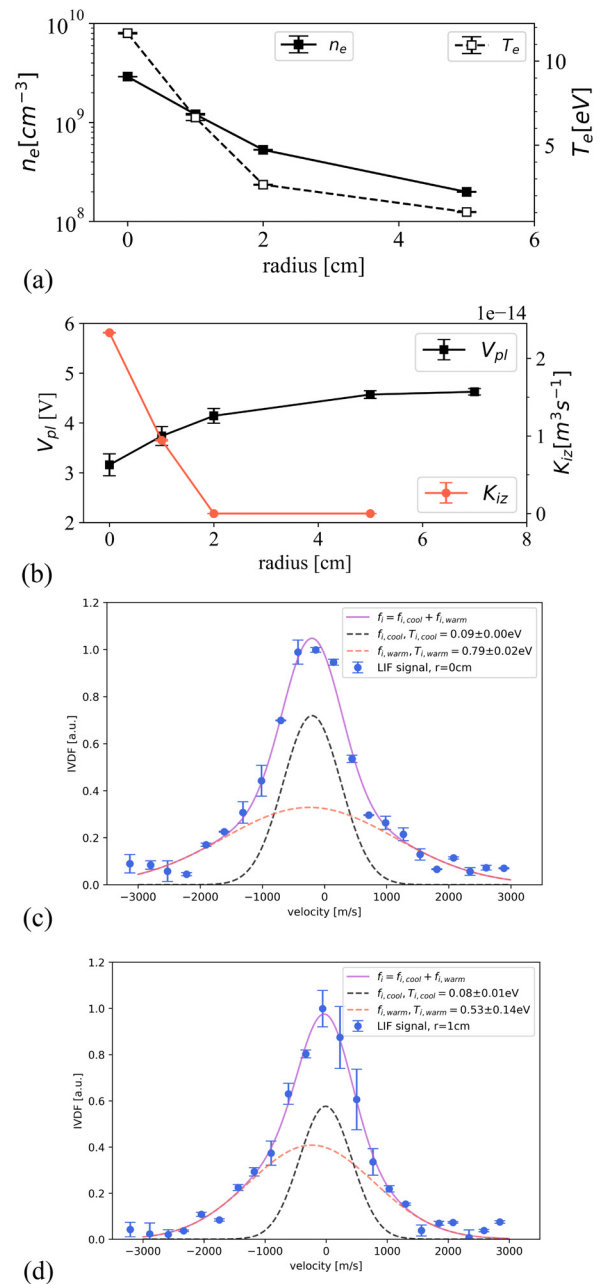
FIG. 2. Plasma properties obtained for the e-beam plasma at the magnetic field of B = 100 G and argon gas pressure of p = 0.1 mTorr: (a) electron density and electron temperature determined by the Langmuir probe, (b) plasma potential determined by emissive probe and ionization rate constant deduced using the measured EEDF, (c) normalized ion velocity distribution functions at $r = 0$ cm, and (d) $r = 1$ cm determined by LIF measurements. Also shown is a least squares fit with a two temperature VDF as the fitting function.

possibility of ion heating mediated by neutral–ion collisions. The LIF setup and transitions used in these experiments are described in Refs. 12, 13, and 17. The results of the argon IVDF measured by LIF are shown in Figs. 2(c) and 2(d). The fitting of IVDF shapes is performed

by a least squares fitting algorithm and indicates the formation of a two-temperature ion velocity distribution. A model function $f_i = f_{i,cool} + f_{i,warm}$, representing a sum of two Maxwellians, was used for the fit. The components of f_i are defined as $f_{i,cool,warm} = a_{i,cool,warm}\exp\left[-\frac{1}{2}m_i(v - v_{i,cool,warm})^2/(kT_{i,cool,warm})\right]$, where m_i is the argon ion mass. The two-temperature fit indicates $T_{i,cool} = 0.1\,\text{eV}$ and $T_{i,warm} = 0.8\,\text{eV}$ at the discharge center $r = 0\,\text{cm}$ and $T_{i,cool} = 0.1\,\text{eV}$ and $T_{i,warm} = 0.5\,\text{eV}$ at $r = 1\,\text{cm}$.

The production of the cold ions, $f_{i,cool}$, may be attributed to the local formation of relatively cold ions during electron impact ionization of neutrals by the e-beam [Fig. 2(b)]. LIF measurements of the neutral argon VDF indicate that the neutral argon temperature is close to room temperature, $T_n \approx 0.026\,\text{eV}$. Because the neutral atoms are much colder than the ions, the neutral population is not responsible for ion heating and there is apparently an ion heating that takes place in the plasma bulk. The production of the warm ions, $f_{i,warm}$, may be attributed to the acceleration of ions inward by the radial potential well. Newly generated ions are born in the region $r = 0$–$1.5\,\text{cm}$, corresponding to the radial extent of the region for which the ionization rate constant is nonzero [Fig. 2(b)]. These ions will be accelerated inward by the $\sim 1\,\text{V}$ potential drop between $r = 0$–$1.5\,\text{cm}$ and will gain $\sim 1\,\text{eV}$ kinetic energy in the radial direction as they reach the center of the discharge, generating the warm ion population at $r = 0\,\text{cm}$ [Fig. 2(c)]. The warm ion population at $r = 1\,\text{cm}$ is similarly produced by ions born for $r = 1$–$1.5\,\text{cm}$. Ions born at $r = 1.5\,\text{cm}$ are accelerated by the corresponding $\sim 0.5\,\text{V}$ potential drop toward $r = 1\,\text{cm}$, gaining $\sim 0.5\,\text{eV}$ kinetic energy [Fig. 2(d)]. Ions born on the radially opposite (antipodal) side of the well will also be able to reach $r = 1\,\text{cm}$, resulting in a symmetric IVDF. Notably, ions born at rest in the region $r < 1\,\text{cm}$ are trapped by the well and will not be able to reach $r = 1\,\text{cm}$.

The measured values of the electron and ion temperatures, the electron density, and the plasma potential can be used to determine the radial flux of electrons and ions in the plasma. We assume for the ion cross field transport, ion–neutral atom collisions are dominant over other collisions, such as Coulomb and charge exchange (CEX) collisions, as supported by the calculated collision frequencies shown in Table I. The ion–neutral collision frequency ν_{in} and axial ion loss frequency $\nu_{i,loss}$, which constitute the axial and radial loss of ions from the potential well, are additionally much less than the ballistic oscillation frequency of trapped ions in the potential well, $\Omega_r = \sqrt{2eE_r/m_i r_{well}} \approx 150\,\text{kHz}$, where $r_{well} = 1\,\text{cm}$ is the approximate radial length scale of the potential well.[9] Thus, an ion born in the electrostatic potential well is radially trapped until a collision with a neutral atom causes the ion to diffuse out of the well or until it is lost on the

side walls. In the region of the potential well, the ion gyro radius is $r_{Li} = m_i v_{thi}/eB \approx 2\,\text{cm}$, and so ions are marginally non-magnetized. Because the ion cyclotron frequency f_{ci} and ion–neutral collision frequencies are comparable, $f_{ci} = \frac{eB}{2\pi m_i} = 4\,\text{kHz} \sim \nu_{in}$, ions may undergo an azimuthal precession in the potential well.

For the region $r \geq 1\,\text{cm}$, the EEDF is nearly Maxwellian, and the electron flux across the magnetic field and the flux of unmagnetized ions in this region can be described by electron and ion fluids, respectively,

$$\Gamma_e(\alpha) = -\mu_{e\perp}(\alpha)n_e E - D_{e\perp}(\alpha)\nabla n_e,$$
$$\Gamma_i = \mu_i n_i E - D_i \nabla n_i, \qquad (2)$$

where $\mu_{e\perp}$ and $D_{e\perp} = \frac{kT_e}{e}\mu_{e\perp}$ are the electron cross field mobility and diffusion coefficients, respectively, μ_i and $D_i = \frac{kT_i}{e}\mu_i$ are the ion mobility and diffusion coefficients, respectively, and $E = -\partial V_{pl}/\partial r$ is the radial component of the electric field.

To evaluate electron transport across the magnetic field, an effective electron transport frequency accounting for electron–neutral collisions and fluctuation-based scattering of electrons (so-called anomalous cross field transport) can be expressed as[21]

$$\nu_{at} = \nu_{en} + \alpha\omega_{ce}, \qquad (3)$$

where $\nu_{en} = n_g\sigma_{en}v_{the}$ is the electron–neutral collision frequency, $\omega_{ce} = eB/m_e$ is the electron cyclotron frequency, with the electron thermal velocity $v_{the} = \sqrt{k_B T_e/m_e}$, and σ_{en} is the effective momentum transfer cross section for electron collisions with Ar atoms evaluated at the mean energy of bulk electrons equal to $\frac{3}{2}kT_e$. In Eq. (3), the parameter α is a semi-empirical parameter characterizing the relative significance of classical to anomalous collisions, which is usually determined from experiments (e.g., $\alpha > 0$ corresponds to anomalous, fluctuation-based diffusion,[21] and $\alpha = 0$ corresponds to classical collisional transport). In the e-beam plasma considered here, the electrons are magnetized, $\frac{r_{Le}}{R_{ch}} \gg 1$ and $\frac{\omega_{ce}}{\nu_{en}} \gg 1$, where r_{Le} is the electron gyro-radius. Under such conditions, the parameter α represents the inverse of an effective electron Hall parameter. The expression for the semiempirical electron cross field mobility is then given by

$$\mu_{e\perp}(\alpha) = \left(\frac{e}{m_e\nu_{at}(\alpha)}\right)\frac{1}{1 + \omega_{ce}^2/\nu_{at}(\alpha)^2}. \qquad (4)$$

Assuming the ion mobility in the radial direction is dominated by ion–neutral collisions, the ion mobility in the radial direction is

$$\mu_i = \frac{e}{m_i\nu_{in}} = \frac{e}{m_i(kT_i/m_i)^{0.5}n_g\sigma_{in}}. \qquad (5)$$

TABLE I. Frequencies relevant to the transport of ions in the discharge. Ar ion–neutral collision rate: $\nu_{in} = n_g\sigma_{in}v_{thi}$ with ion thermal velocity $v_{thi} = \sqrt{kT_i/m_i}$, ion–neutral momentum transfer cross section $\sigma_{in} = 1.2 \times 10^{-18}\,\text{m}^2$,[18] ion temperature near discharge center $T_i = 0.8\,\text{eV}$ [Fig. 2(c)], and gas density $n_g = p/kT_g$ with neutral pressure $p = 0.1\,\text{mTorr}$ and neutral temperature $T_g = 300\,\text{K}$. Ar ion–neutral charge exchange (CEX) collision rate: $\nu_{in}^{CEX} = n_g\sigma_{CEX}v_{thi}$ with collision cross section for $\sigma_{CEX} = 6.5 \times 10^{-19}\,\text{m}^2$.[19] Ion–ion Coulomb collision rate: $\nu_{ii} = (\ln\Lambda e^4 n_i)/(12\pi^{3/2}\varepsilon_0^2\sqrt{m_i}T_i^{3/2})$ with Coulomb logarithm $\ln\Lambda \approx 16$, vacuum permittivity ε_0,[20] and ion density at discharge center $n_i = 3 \times 10^9\,\text{cm}^{-3}$ assuming quasineutrality $n_i \approx n_e$ [Fig. 2(a)]. Axial ion loss rate to cathode: $\nu_{i,loss} = v_{thi}/(L_{ch}/2)$.

	ν_{in}	ν_{in}^{CEX}	ν_{ii}	$\nu_{i,loss}$	Ω_r	f_{ci}
Values (kHz)	5	3	0.1	6	150	4

The current collected by the cathode and collector, I_d and I_{col}, are independently measured. The discharge current is measured to be $I_d = 94$ mA. From these current measurements, it is determined that a fraction $x = I_{col}/I_d = 40\%-70\%$ of the discharge current is conducted axially from the collector to cathode. This indicates that the remaining fraction $(1 - x) = 30\%-60\%$ of discharge current is conducted radially between the chamber walls and the electron beam region at the center of the plasma (Fig. 1) connected to the cathode. Positive discharge current is conducted radially inward, i.e., in the $-\hat{\mathbf{r}}$ direction. Under the assumptions of quasineutrality ($n_i \approx n_e$) and uniform longitudinal distribution of the cross field current, the steady state balance for the radial component of the discharge flux Γ_r is given by

$$\mathbf{\Gamma_d} \cdot \hat{\mathbf{r}} = -\Gamma_r = -\frac{I_d(1-x)}{eA_r} = \Gamma_i - \Gamma_e(\alpha), \tag{6}$$

where $A_r = 2\pi r L_{ch}$ is the area of a cylindrical shell of radius r and length L_{ch}, through which radial current is conducted. The electron and ion flux equations given by Eqs. (2) can be used to express Eq. (6) in the following form:

$$-\Gamma_r = +\Gamma_{i,\text{dif.}}(T_i) - \Gamma_{i,\text{mob.}}(T_i) - \Gamma_{e,\text{mob.}} - \Gamma_{e,\text{dif}}, \tag{7}$$

with signs chosen conveniently such that the terms $\Gamma_{j,\text{mob.}}$ and $\Gamma_{j,\text{dif.}}$, the mobility, and diffusion fluxes of species j, respectively, are positive for $\mathbf{E} \cdot \hat{\mathbf{r}} < 0$ and $\nabla n_e \cdot \hat{\mathbf{r}} < 0$ (corresponding to the experimentally measured conditions). Explicitly, in Eq. (7), $\Gamma_{i,\text{mob.}} = -\mu_i n_e E$, $\Gamma_{i,\text{dif.}} = -\mu_i \frac{kT_i}{e} \nabla n_e$, $\Gamma_{e,\text{mob.}} = -\mu_{e\perp} n_e E$, $\Gamma_{e,\text{dif.}} = -\mu_{e\perp}\left(\frac{kT_e}{e}\nabla n_e\right)$, and $\Gamma_d = \frac{I_d(1-x)}{eA}$. Importantly, the only flux term that produces an outward directed ($+\hat{\mathbf{r}}$ direction) current density is the ion diffusion flux, $\Gamma_{i,\text{dif.}}$, i.e., the ion backflux toward the anode.

According to Eq. (5), the ion mobility follows the scaling $\mu_i \propto T_i^{-1/2}$. Hence, the ion mobility flux scales as $\Gamma_{i,\text{mob.}} = \mu_i n_e E \propto T_i^{-1/2}$, while the diffusive ion backflux scales as $\Gamma_{i,\text{dif.}} = \frac{kT_i}{e}\mu_i \nabla n_e \propto T_i^{1/2}$. Thus, Eq. (7) is quadratic in the ion thermal velocity . Solving the quadratic equation in terms of measured parameters and keeping the physical root, we find an expression for the ion temperature that produces a sufficient diffusive ion backflux to satisfy the current continuity,

$$\sqrt{\frac{kT_i}{m_i}} = \frac{(-\Gamma_r + \Gamma_e(\alpha)) + \sqrt{(-\Gamma_r + \Gamma_e(\alpha))^2 + \frac{4}{m_i}(\nabla n_e)(en_e E)\lambda_{in}^2}}{-2\nabla n_e \lambda_{in}}. \tag{8}$$

Equation (8) expresses the ion temperature in terms of the measured plasma parameters (Γ_r, n_e, T_e, E) and a semiempirical electron flux $\Gamma_e(\alpha)$. The functional form indicates the predicted ion temperature is monotonically increasing with electron flux. Therefore, a conservative estimate (lower bound) on the ion temperature is obtained for the case of the minimum electron flux. Examining Eqs. (3) and (4), the cross field electron mobility $\mu_{e\perp}(\alpha)$ vanishes in the limit of $\alpha \to \infty$ such that

$$\lim_{\alpha \to \infty} \Gamma_e(\alpha) = 0. \tag{9}$$

Additionally, in the limit $\nu_{en} \to 0$, the classical cross field mobility $\mu_{e\perp}(0)$ also vanishes such that

$$\lim_{\alpha \to 0} \Gamma_e(\alpha) = 0, \tag{10}$$

whereby the $\alpha = 0$ case also serves to conservatively estimate a lower bound of the ion temperature.

Figure 3 compares spatial profiles of the determined ion temperature profiles estimated using the experimental data with the ion temperatures deduced from LIF measurements. A good agreement between the estimated and measured warm ion temperatures is found for the classical collisional electron transport and anomalous transport cases with $\alpha = 0$ and $\alpha = 50$, respectively. In both cases of $\alpha = 0$ and $\alpha = 50$, the electron flux as determined by Eq. (2) is negligible compared to the ion mobility and ion diffusion fluxes. Thus, the radial current conduction is dominated by a trade-off between the ion mobility and the ion diffusion.

There are at least three points in this work regarding the heating and transport of ions that merit further investigation: (i) radial ion mobility was assumed to be dominated by trapped ions undergoing ion–neutral collisions and escaping the potential well. However, the effect of ion precession due to E × B fields on radial ion transport is outside of the scope of this Letter and should be addressed in future work. (ii) It was also proposed in this paper that ions gain energy by radial acceleration by the potential well, but there may be alternative ion heating mechanisms present due to plasma instabilities. Ions born on radially antipodal sides of the potential well will be accelerated by the electric field to form counterpropagating ion populations at the central region of the well. Anomalous ion heating may be attributed to the growth of a lower hybrid drift instability caused by these counterpropagating ion populations near the discharge center.[22] (iii) Another possible ion heating mechanism may be due to the coupling of the e-beam injected from the cathode with the bulk plasma, Langmuir waves, and ion acoustic waves, leading to the onset of a beam-plasma
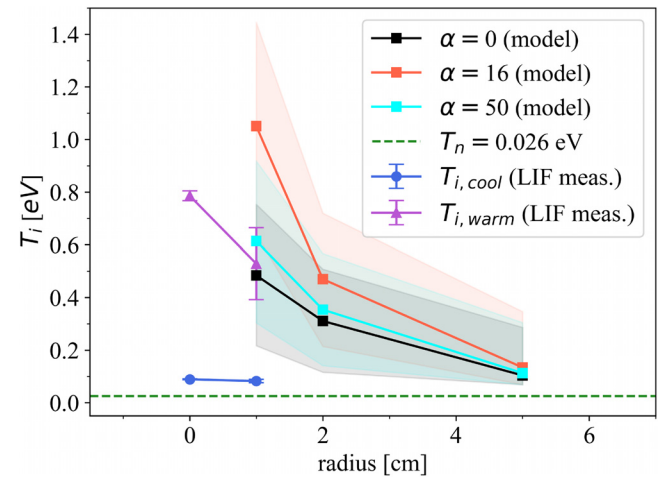

FIG. 3. Radial dependence of ion temperature of cool ($T_{i,cool}$) and warm ($T_{i,warm}$) ion populations determined by LIF. Also plotted is the ion temperature determined by the radial current continuity model [Eq. (8)], for anomalous coefficient cases $\alpha = 0$, 16, and 50. The shaded regions indicate the uncertainty in the ion temperature determined by the model. This uncertainty is caused by the experimental uncertainty in the measured plasma potential radial profile [Fig. 2(b)]. The neutral argon temperature T_n is also plotted for reference (green dashed line).

instability.[23] The exact ion heating mechanism in the discharge should be investigated in future works.

In conclusion, our measurements revealed the presence of a warm group of ions responsible for generating a radial ion flux toward the peripheral plasma region of an e-beam generated E × B plasma source. The generation of the warm ion population may be attributed to the acceleration of ions born on either side of the radial potential well, while the generation of the cool population may be due to the local production of ions from cool neutrals. However, the warm ions may diffuse in the direction opposite to the electric field. Indeed, ions are heated enough to generate a diffusive ion backflux toward the periphery of the plasma to ensure current continuity and plasma quasineutrality. The ion kinetics and radial charge transport demonstrated in this work can have practical implications for low-damage material processing. In material processing scenarios, the diffusion of warm ions to the wafer is responsible for the ambipolar plasma flow to the substrate.

AUTHOR DECLARATIONS
Conflict of Interest

The authors have no conflicts to disclose.

Author Contributions

Nirbhav Singh Chopra: Conceptualization (equal); Data curation (lead); Formal analysis (lead); Investigation (equal); Validation (equal); Writing – original draft (lead); Writing – review & editing (equal). **Ivan Romadanov:** Data curation (equal); Formal analysis (equal); Investigation (equal); Writing – original draft (supporting); Writing – review & editing (supporting). **Yevgeny Raitses:** Conceptualization (lead); Formal analysis (equal); Supervision (lead); Writing – review & editing (supporting).

DATA AVAILABILITY

The data that support the findings of this study are available from the corresponding author upon reasonable request.

REFERENCES

[1]F. Zhao, Y. Raitses, X. Yang, A. Tan, and C. G. Tully, "High hydrogen coverage on graphene via low temperature plasma with applied magnetic field," Carbon **177**, 244–251 (2021).

[2]S. G. Walton, D. R. Boris, S. C. Hernández, E. H. Lock, T. Petrova, G. M. Petrov, and R. F. Fernsler, "Electron beam generated plasmas for ultra low T_e processing," ECS J. Solid State Sci. Technol. **4**(6), N5033–N5040 (2015).

[3]D. B. Zolotukhin, V. A. Burdovitsin, and E. M. Oks, "On the role of secondary electrons in beam plasma generation inside a dielectric flask by fore-vacuum plasma-cathode electron source," Phys. Plasmas **24**(9), 093502 (2017).

[4]R. F. Fernsler, W. M. Manheimer, R. A. Meger, J. Mathew, D. P. Murphy, R. E. Pechacek, and J. A. Gregor, "Production of large-area plasmas by electron beams," Phys. Plasmas **5**(5), 2137–2143 (1998).

[5]W. M. Manheimer, R. F. Fernsler, M. Lampe, and R. A. Meger, "Theoretical overview of the large-area plasma processing system (LAPPS)," Plasma Sources Sci. Technol. **9**, 370–386 (2000).

[6]S. Rauf, A. Balakrishna, A. Agarwal, L. Dorf, K. Collins, D. R. Boris, and S. G. Walton, "Three-dimensional model of electron beam generated plasma," Plasma Sources Sci. Technol. **26**(6), 065006 (2017).

[7]L. Dorf, J.-C. Wang, S. Rauf, Y. Zhang, A. Agarwal, J. Kenney, K. Ramaswamy, and K. Collins, "Atomic precision etch using a low-electron temperature plasma," Proc. SPIE **9782**, 97820J (2016).

[8]E. Rodríguez, V. Skoutnev, Y. Raitses, A. Powis, I. Kaganovich, and A. Smolyakov, "Boundary-induced effect on the spoke-like activity in E × B plasma," Phys. Plasmas **26**(5), 053503 (2019).

[9]Y. Sakawa, C. Joshi, P. K. Kaw, F. F. Chen, and V. K. Jain, "Excitation of the modified Simon–Hoh instability in an electron beam produced plasma," Phys. Fluids B **5**(6), 1681–1694 (1993).

[10]J. W. Koo and I. D. Boyd, "Modeling of anomalous electron mobility in Hall thrusters," Phys. Plasmas **13**(3), 033501 (2006).

[11]J. P. Boeuf and M. Takahashi, "New insights into the physics of rotating spokes in partially magnetized E × B plasmas," Phys. Plasmas **27**(8), 083520 (2020).

[12]G. D. Severn, D. A. Edrich, and R. McWilliams, "Argon ion laser-induced fluorescence with diode lasers," Rev. Sci. Instrum. **69**(1), 10–15 (1998).

[13]A. M. Keesee, E. E. Scime, and R. F. Boivin, "Laser-induced fluorescence measurements of three plasma species with a tunable diode laser," Rev. Sci. Instrum. **75**(10), 4091–4093 (2004).

[14]M. A. Lieberman and A. J. Lichtenberg, *Principles of Plasma Discharges and Materials Processing*, 2nd ed. (Jon Wiley & Sons, Inc., Hoboken, NJ, 2005).

[15]B. F. Kraus and Y. Raitses, "Floating potential of emitting surfaces in plasmas with respect to the space potential," Phys. Plasmas **25**(3), 030701 (2018).

[16]H. C. Straub, P. Renault, B. G. Lindsay, K. A. Smith, and R. F. Stebbings, "Absolute partial and total cross sections for electron-impact ionization of argon from threshold to 1000 eV," Phys. Rev. A **52**(2), 1115–1124 (1995).

[17]I. Romadanov and Y. Raitses, "A confocal laser-induced fluorescence diagnostic with an annular laser beam," Rev. Sci. Instrum. **94**(7), 073002 (2023).

[18]A. V. Phelps, "Cross sections and swarm coefficients for nitrogen ions and neutrals in N_2 and argon ions and neutrals in Ar for energies from 0.1 eV to 10 keV," J. Phys. Chem. Ref. Data **20**(3), 557–573 (1991).

[19]B. J. Nichols and F. C. Witteborn, *Measurements of Resonant Charge Exchange Cross Sections in Nitrogen and Argon between 0.5 and 17 EV* (NASA, 1966).

[20]R. Fitzpatrick, *Plasma Physics: An Introduction*, 2nd ed. (CRC Press, Boca Raton, 2022).

[21]J. P. Boeuf and L. Garrigues, "Low frequency oscillations in a stationary plasma thruster," J. Appl. Phys. **84**(7), 3541–3554 (1998).

[22]I. G. Mikellides and A. Lopez Ortega, "Growth of the lower hybrid drift instability in the plume of a magnetically shielded Hall thruster," J. Appl. Phys. **129**(19), 193301 (2021).

[23]H. Sun, J. Chen, I. D. Kaganovich, A. Khrabrov, and D. Sydorenko, "Physical regimes of electrostatic wave-wave nonlinear interactions generated by an electron beam propagating in a background plasma," Phys. Rev. E **106**(3), 035203 (2022).